Mettl5 coordinates protein production and degradation of PERIOD to regulate sleep in *Drosophila*

Xiaoyu Wu[1#], Xingzhuo Yang[1#], Tiantian Fu [1#], Yikang S. Rong[2], Juan Du[1*]

1 Department of Entomology, MOA Key Lab of Pest Monitoring and Green Management, College of Plant Protection, China Agricultural University, Beijing 100193, China

2 MOE Key Lab of Rare Pediatric Diseases, Hengyang College of Medicine, University of South China, Hengyang, China

[*]Correspondence author: Juan Du, dujuan9981@cau.edu.cn

[#] These authors contribute equally to this work.

Summary

Sleep is crucial for animal physiology, primarily governed by the brain, and disruptions are prevalent in various brain disorders. *Mettl5*, associated with intellectual disability (ID) often accompanied by sleep disturbances, remains poorly understood in its role causing these disorders. Previous research demonstrated that Mettl5 forms a complex with Trmt112, influencing rRNA methylation. In our study, we explored sleep phenotypes due to *Drosophila Mettl5* mutations. Rescue experiments pinpointed *Mettl5*'s predominant role in neurons and glia marked by *Mettl5*-Gal4 in sleep regulation. Notably, a *Trmt112* mutation mirrored these sleep disturbances, implicating translational regulation via the Mettl5/Trmt112 complex. Subsequent RNA-seq and Ribo-seq analyses unveiled downstream events from *Mettl5*^{1bp} mutations, revealing altered expression levels of proteasome components and Clock genes. Rescue experiments confirmed that the net increased PERIOD protein is responsible for the sleep phenotype. This investigation sheds light on ribosome, clock genes, and proteasome interplay in sleep regulation, underscoring protein synthesis and degradation's integrative role. These findings could potentially provide an example of *in vivo* study of the function of rRNA methylation, expand our understanding of the role of protein homeostasis in sleep and inspire explanations on the ID related sleep phenotypes.

Key words: *Mettl5*, rRNA methyltransferase, proteasome, Clock genes, sleep

Introduction

Sleep serves critical functions for animals. Investigating the molecular mechanisms underlying sleep holds profound importance for both fundamental research and practical applications. While previous studies have identified several sleep regulators (*Du et al., 2021*), gaps persist in comprehending fundamental cellular processes like protein synthesis and degradation in relation to sleep.

Evidence suggests a correlation between sleep regulation and protein synthesis and degradation, both of which control protein levels dynamically. Protein synthesis is particularly active during sleep (*Lyons et al., 2023*). Sleep deprivation targets translational initiation, impacting this process (*Costa et al., 2019*). The proteasome, crucial for ubiquitination-mediated protein degradation, plays a key role in synapse homeostasis by modulating ribosomal components (*Costa et al., 2019*), thereby influencing synaptic function. Additionally, proteasome components exhibit a circadian expression pattern at the transcriptional level in human cells (*Desvergne et al., 2016*). A recent study in *Drosophila* showed that mutation of a proteasome component alters sleep patterns (*Fernández et al., 2020*). The roles of protein synthesis and degradation in sleep regulation, as well as their interactions, remain open questions.

Several factors influencing proteasome assembly and subunit transcription have been identified (*Kapetanou et al., 2022*). However, there remains a significant gap in research regarding the translational control of proteasome subunits. Furthermore, it has been reported that proteasome inhibition can lead to changes in ribosome function (*Galimberti et al., 2016; Costa et sl., 2019; Palanca et al., 2014*). An open question persists as to whether the proteasome is regulated by the status of the translation machinery. Exploring this relationship could provide deeper insights into the interplay between proteasome function and translation.

Drosophila Mettl5 exhibits 18S ribosomal RNA m^6A methyltransferase activity (*Leismann et al., 2020*). In both *Drosophila* and human, Mettl5 interacts with Trmt112 to facilitate this function (*Leismann et al., 2020; van Tran et al., 2019*) Depletion of *Mettl5* results in the absence of m^6A modification on 18S rRNA, yet does not affect rRNA maturation. The loss of *Mettl5*-mediated m^6A modification influences fly orientation. In mammalian cells, this gene was found mediating 18S rRNA N6-methyladenosine (m^6A) modification and controlling stem cell fate determination and neural

function (*Wang et al.*, *2020*). However, it remains intriguing whether *Mettl5* impacts global or transcript-specific translation profile, especially in tissues *in vivo* instead of cell lines. Furthermore, *Mettl5*, associated with intellectual disability (ID) often accompanied by sleep disturbances, remains poorly understood in its role causing these disorders. Thus, test whether the loss of *Mettl5* loss affect behavior such as sleep in *Drosophila* would shed light on this problem.

We discovered that *Mettl5* regulates sleep. To investigate the underlying mechanism, we used RNA-seq and Ribo-seq to reveal downstream events associated with *Mettl5* mutations. We identified multiple clock genes and proteasome components regulated by *Mettl5*, suggesting a coordinated regulation of protein production and degradation, crucial for protein homeostasis. Further experiments showed that the protein level of Period was upregulated, contributing to the sleep phenotype. This study highlights how ribosome defects can impact proteasome function, demonstrating a mechanism that coordinates protein degradation with protein production. Additionally, by mapping the genome-wide profile of an rRNA methylation modifier, this study offers insights into the gene-specific roles of ribosome function.

Results

Mettl5 is a regulator of *Drosophila* sleep

Mettl5 is predicted to have a N6 adenine specific nucleic acids methylase domain. In order to study the function of this gene in sleep regulation, we generated mutants by CRISPR-Cas9 deletion. Allele $Mettl5^{1bp}$, which deleted 1bp in the coding region results in a truncated version (Figure 1A) and down regulation of *Mettl5* at mRNA level (Figure 1B). Another allele $Mettl5^{9bp}$, which results in 3 amino acids deleted version of *Mettl5* (Figure 1A) does not cause significant change at mRNA level (Figure 1B). We found that the heterozygous $Mettl5^{1bp}$ mutation results in decreased total sleep during the night time, which is resulted from the effect of decrease of sleep at early night time (Figure 1C-F). The sleep curve showed a significant down regulation of sleep at ZT12 to ZT16 (Figure 1C). The calculation of the awake percentage at ZT14 indicated a significant increase of this parameter in $Mettl5^{1bp}$ (Figure 1G). In addition, *Mettl5* expression was significantly up regulated during the sleep recovery period after mechanical sleep deprivation (Figure 1M-N). Consistently, the sleep recovery was down regulated in the *Mettl5* mutant (Figure 1O), indicating the sleep homeostasis was affected by *Mettl5*.

In conclusion, the truncated mutation of *Mettl5* resulted in sleep phenotypes.

To verify the specificity of the sleep phenotype caused by *Mettl5*^{1bp}, we did the rescue experiment. The results showed that supplying of one copy of *Mettl5* to *Mettl5*^{1bp} rescued the sleep phenotype in sleep amount and awake percentage at ZT14 (Figure 1H-L). These results verified the specificity of the phenotype.

To verify in which cells did *Mettl5* function for the sleep phenotype, we checked the expression pattern of *Mettl5*-Gal4. The results indicated that a portion of the *Mettl5*-Gal4 marked cells colocalized with Repo antibody staining (Figure S1A-C). Another portion of the *Mettl5*-Gal4 marked cells colocalized with ELAV antibody staining (Figure S1D-F). In addition, we also tested the climbing ability of *Mettl5* mutation which showed an increase (Figure S1G). The sleep arousal assay also indicated an increased sleep arousal (Figure S1H). Moreover, the lifespan increased in the mutant (Figure S1I).

Mettl5 regulation on _Drosophila_ sleep was dependent on its methyltransferase activity

Previous studies have shown that Mettl5 interacts with Trmt112 to regulate 18S rRNA m^{6}A modification (*Leismann et al., 2020; van Tran et al., 2019*). Consistently, we found that the methylation level in both total and 18S rRNA decreased in heterozygous *Mettl5*^{1bp}. We tested the m^{6}A level using LC-MS/MS experiment. The m^{6}A level decreased in heterozygous *Mettl5*^{1bp} either in both total RNA and 18S rRNA (Figure 2A-B). To investigate the mechanism of *Mettl5* regulation on sleep. We examined the phenotype of *Trmt112* knockdown. We found that the *Mettl5*-Gal4 driven *Trmt112* RNAi resulted in a similar phenotype to *Mettl5*^{1bp} (Figure 2C-G), suggesting that *Mettl5* regulates sleep through its 18S rRNA m^{6}A modification activity. The efficiency of the *Trmt112* RNAi line was tested in previous study (*López-Varea et al., 2021*). More important, we performed a rescue experiment with a mutated form of *Mettl5* that lacks the NPPF amino acids required for its methyltransferase activity. We observed that this mutant *Mettl5* failed to rescue the sleep phenotype caused by *Mettl5*^{1bp} (Figure 2H-L). These results collectively indicated that the methyltransferase activity of *Mettl5* is essential for its role in *Drosophila* sleep.

RNA-seq and Ribo-seq revealed the downstream gene profile of _Mettl5_

To better understand the downstream events of *Mettl5*, we analyzed RNA-seq and Ribo-seq data to

evaluate the effects of *Mettl5*^{1bp} on gene expression. The analysis of the RNA-seq and Ribo-seq data followed by the Principal Coordinates Analysis (PCoA) showed a clear separation between the two groups (Figure S2A, B, D, E). High correlation was found between the three biological repeats for each sample (Figure S2C, F), indicating that RNA-seq and Ribo-seq quality was high. Differentially expressed gene analysis of RNA-seq showed that 1053 genes ($|\log_2$ (Fold Change) $| \geq 1$ & $p^{adj} < 0.05$) were significantly changed at the transcription level (Figure 3A), including 217 up-regulated and 836 down-regulated genes (Figure 3B, Table S1). Differentially expressed gene analysis of Ribo-seq showed that 258 genes were significantly changed at the translation level ($|\log_2$ (Fold Change) $| \geq 0.265$ & $p^{adj} < 0.05$), including 149 up-regulated and 150 down-regulated genes (Figure 3C, Table S1). The top 100 differentially expressed genes found in RNA-seq (Figure S3A) and Ribo-seq (Figure S3B) were shown in a heatmap generated according to the rlog transformed values.

To explore the biological implication of the differentially expressed genes at transcriptional and translational levels, Gene ontology (GO) enrichment was performed. At the transcriptional level (Figure S4A, C), the most significantly enriched biological processes GO terms were related to cellular response, biosynthetic process and metabolic process, such as cellular response to chemical stimulus, small molecule biosynthetic process, fatty acid metabolic process (Figure S4A). Several term related gene network also be shown (Figure S4C). At the translation level (Figure S4B, D), the most significantly enriched biological processes GO terms were related to organic acid metabolic process, amino acid metabolic process, lipid catabolic process, cellular respiration, and transport mechanisms. Additionally, we found prominent terms related to circadian rhythm genes, including circadian regulation of gene expression and entrainment of the circadian clock (Figure S4B, D).

The GO results usually contain a long list of enriched terms that have highly redundant information and are difficult to summarize. So, we performed a simplify Enrichment analysis that visualizes the summaries of clusters by word cloud for the GO enrichment result at transcriptional and translational levels. We found that the main biological process was metabolic, the response signaling stimulus; the development of wing disc; imaginal et.al system; the homeostasis and transport for ion-channel; the cycle of cytokinesis and transition in transcriptional significant DEG (Figure S5A). Except for the above main biological progress, the significant translated genes also showed enrichment

for the sleep wake, cycle related behavior circadian rhythm and neuron death (Figure S5D). For cellular components, the main enrichments are chromosome structures, complexes, membranes, and vesicles (Figure S5B). Molecular functions primarily include enzymatic activities, ion and protein binding, receptor activities, and transcription processes (Figure S5C). The RNA-seq results are very similar to the Ribo-seq results (Figure S5E-F).

Gene Set Enrichment Analysis (GSEA) revealed pathways that were enriched in differentially expressed genes at both transcriptional and translational levels. As the significant genes enrichment analysis will lose some key important message which are caused by unreasonable screening parameters, these gene sets ranked by $\log_2$fold-change only (not screened by p values) were considered in the GSEA. The GSEA-GO and GSEA-KEGG enrichment results of the transcriptional and translational genes were sorted according to the Normalized enrichment score (NES) value (Figure S6A-D). We found some important pathway such as proteasome pathway that were suppressed at both transcriptional and translational levels (P.adjust<0.05) (Figure 3E, I). Arginine and proline metabolism and insect hormone biosynthesis were significantly affected at transcriptional level (P.adjust<0.05) (Figure 3D, G). While, fatty acid degradation, Phosphonate and Phosphinate metabolism,etc. were significantly affected at translational level (P.adjust<0.05) (Figure 3H-K).

In particular, GSEA analysis showed some interesting results. Gene ontology analysis (GSEA-GO) of the GSEA gene set showed a suppression of mitochondria related activities both at transcriptional and translational levels (Figure S6A, C). The aromatic amino acid metabolic and catabolic process were activated at transcriptional level (Figure S6A). While, the signaling receptor, molecular transducer activity related term was activated at translational level (Figure S6C). The KEGG analysis (GSEA-kegg) indicated that at transcriptional level, we found that the pathway Pentose and glucuronate interconversions, Insect hormone biosynthesis, Drug metabolism - cytochrome P450 et.al were activated (Figure S6B). While, arginine and proline metabolism, Proteasome, Phagosome, Oxidative phosphorylation etc. pathway were suppressed (Figure S6B). *Mettl5*^{1bp} mainly affected the physiological activities through activating Phototransduction, Phosphonate metabolism, Glycosylphosphatidylinositol (GPI)-anchor biosynthesis etc. pathways at translational level (Figure S6D). At the same time, it suppressed Peroxisome, amino acid metabolism, Fatty acid degradation,

169 proteasome etc. pathways at the translational level (Figure S6D).

170 To better understand the correlation between transcription and translation levels, we performed
171 correlation analysis of differentially expressed genes based on fold change of DEGs (Figure 3L). we
172 found 977 genes which had opposite tendency of change at transcriptional vs. translational levels, 24
173 genes which had same tendency of change at transcriptional *vs.* translational levels., 240 genes which
174 changed only at translational level and 3309 genes which changed only at transcriptional level. These
175 four gene clusters were analyzed by enrichment analysis (Figure S7A-H). The expression of important
176 clock gene *Clk*, *tim* etc. were significantly changed at both transcriptional and translational levels
177 (Figure 3L).

178 To assess net translation alterations and exclude the effects of transcription changes, we analyzed
179 translation efficiency (TE). We found a change of TE in $Mettl5^{1bp}$ compared to w^{1118} (Figure 3M, Table
180 S1). We obtained 1204 genes that had significantly different TE. We performed GO and KEGG
181 enrichment analysis for these genes. GO enrichment indicated that these genes mainly enriched in
182 amino acid metabolic process and small molecule biosynthetic process etc. (Figure 3N). The KEGG
183 enrichment analysis showed that the main pathway are Glycine, serine and threonine metabolism, one
184 carbon pool by folate, etc. (Figure 3O, P).

185 **Ribo-seq revealed the $Mettl5^{1bp}$ led to changes of some global translation features**

186 Ribo-seq revealed the global translation features in two groups, w^{1118} and $Mettl5^{1bp}$, respectively.
187 The correlation coefficient of TE between the three biological replicates of two groups varied from
188 0.87 to 0.93, indicating a high correlation between the samples of the same genotype (Figure S8A-F).
189 We found that the length of ribosome-protected RNA fragments (RPFs) was approximately 28nt
190 (Figure S10A). The RPFs exhibited a significant 3-nt periodicity. Metagene analysis of individual 28nt
191 reads revealed the distribution of RPFs across the gene locus in w^{1118} and $Mettl5^{1bp}$, respectively (Figure
192 S8, S9). The starting point of translation is 12nt upstream of start-codon and gradually disappears 15nt
193 from stop-codon (Figure S8G-L). RPFs on the metagene plot distribution around the translation start
194 and translation stop site (Figure S9A-F), different coding frames on CDS, 3'-UTR and 5'-UTR,
195 respectively in two groups of samples all showed the periodicity (Figure S9G-L). As expected, all
196 plots show an enrichment of P-sites in the first frame on the coding sequence but not the UTRs, in

197 accord with ribosome protected fragments from protein coding mRNAs (Figure S9G-L).

198 Analysis of the proportion of the different types of open reading frame (ORF) indicated an
199 alteration of the percentage of some types of ORFs. Compared to w^{1118}, we found that *Mettl5*^{1bp} have
200 more overlapped dORFs and less non-overlapped dORFs (Figure S10B). Both of the two groups
201 showed the shorter length of translated uORF compared to untranslated uORF ($P<0.05$) (Figure S10C).
202 *Mettl5*^{1bp} had less dORF and uORF read count (Figure S10D-E). According to the translation potential
203 of uORF, the translated uORF and untranslated uORF can be divided from different sample. Motif
204 analysis was performed on untranslated uORF and translated uORF respectively (Figure S10F-G).

205 Mutation of *Mettl5* altered the codon preference. When comparing the codon occupancy (A-site)
206 correlation between two groups, we find two codons (GAC and GAU) were preferred by *Mettl5*^{1bp} and
207 UCC were preferred by w^{1118} (Figure S10H). The cumulative frequency of these three codons also
208 demonstrated the same trend (Figure S10I-K). The Asp codon GAC and GAU, so we compared the
209 amino acid occupancy of Asp. The result indicated that the frequency of Asp in w^{1118} was significantly
210 enriched in translation (Figure S10L).

211 Metagene plot comparing RPFs between *Mettl5*^{1bp} and w^{1118} revealed the differential translation.
212 The CDS and region around it was divided into 100 equal bins, and the average RPF density was
213 calculated for each bin. The plot visually depicting the differences in ribosome occupancy patterns
214 between *Mettl5*^{1bp} and w^{1118} along the CDS (Figure S10M), around the translation start site (Figure
215 S10N) and around the translation end site (Figure S10O). The plot highlights the divergent ribosome
216 occupancy patterns between *Mettl5*^{1bp} and w^{1118} along the CDS and near the translation start site,
217 indicated potential variations in translation dynamics and disparities in translation initiation (Figure
218 S10M, O).

219 **Clock gene regulatory loop regulating circadian rhythm was affected by *Mettl5*^{1bp}**

220 We found that multiple clock genes had significant changes in both transcriptional and translational
221 levels. *Cry* and *Clock* was significantly upregulated at both transcriptional and translational levels
222 (Figure 4A-B). *Tim, per, vri and pdp1* were significantly downregulated at both transcriptional and
223 translational levels (Figure 4A-B). More important, *per*, *vri,* and *pdp1* were significantly
224 downregulated in translational efficiency (Figure 4C). These genes are components of the clock gene

225 regulatory network which controls the circadian rhythm. The clock neuron morphology was not
226 affected by the mutant (Figure S11).

227 According to the relationship between these genes in the clock regulatory circuit, if Per was
228 downstream of Clock in mediating the function of *Mettl5*, we should have seen the change of both
229 genes to the same direction. However, we detected changes to opposite for Clock and Per. Therefore,
230 we propose that Per was upstream of Clock in mediating the function of *Mettl5.* Then, we examined
231 the protein level of Per. Surprisingly, we found that the protein level of Per was upregulated in the
232 mutant detected by both immunostaining and western blot (Figure 4D-G). This is confirmed by the
233 circadian rhythm phenotype showed by *Mettl5* mutant, which showed a significant increased period
234 length (Table 1). An increased period length was reported in previous case of inactive kinase activity
235 which results in a stabilized Period (*Philpott et al., 2023*). Consistently, genetic evidence indicated
236 that both of *Clock* and *Per* genes were downstream of *Mettl5*, because the double mutant showed the
237 phenotype of clock genes (Figure 4H-M, Table 1). This result indicated that other mechanism
238 regulating Per protein was affected by $Mettl5^{1bp}$.

239 Then we ask what's the factors mediated Per protein level changes in *Mettl5* mutant. By examining
240 the RNA-seq, Ribo-seq data and translation efficiency, we found that multiple components of the
241 proteasome pathways were significantly downregulated in $Mettl5^{1bp}$ (Figure 3E, I, 4N). Based on the
242 above results, we proposed a working model in which *Mettl5* directly regulates proteasome, Per and
243 Clock in transcription and translation. The proteasome regulates Per at post translational level. And in
244 turn Per inhibits Clock at protein level. As a result, in $Mettl5^{1bp}$, the down regulation of proteasome
245 results in the upregulation of Per protein and as a result up regulation of Clock protein activity and its
246 downstream gene transcription (Figure 5).

247 **The axon complexity was affected by $Mettl5^{1bp}$**

248 Previous results have indicated a close correlation between sleep need and synaptic complexity
249 (*Bushey et al., 2011*). Moreover, it has been observed that synaptogenesis stimulates proteasome
250 activity in axons (*Costa et al., 2019*). Considering the loss of sleep rebound after deprivation and the
251 expression level changes of proteasome subunits resulting from $Mettl5^{1bp}$, we were interested in
252 investigating whether synaptic complexity is affected.

To quantify synaptic complexity, we employed a method previously reported (*Bushey et al., 2011*). *Syt*-GFP, a protein product that colocalizes with native synaptic vesicles, was used to visualize changes in presynaptic morphology. As controls, UAS-*Fmr1* and *Fmr1* mutation were utilized, resulting in a decrease and increase of *syt*-eGFP, respectively (Figure 6A-C). Interestingly, we found that the *Mettl5*^{1bp} led to an increase in *syt*-eGFP staining in presynaptic terminals (Figure 6D).

Discussion

In this study, we found that *Mettl5*, a previously identified rRNA methylase, regulates sleep through its RNA methylation activity. RNA-seq and Ribo-seq of the *Mettl5*^{1bp} identified downstream genes of *Mettl5* at transcriptional and translational levels. Further study identified Mettl5 can affect clock gene network and proteasome pathway which mediated *Mettl5* regulation of sleep. By elucidated the molecular mechanism for Mettl5 function on sleep, this study highlighted an integrative role of protein synthesis and degradation in sleep regulation. The Ribo-seq analysis in this study indicated that global features of translation, such as uORF translation efficiency and codon choices, were affected in the *Mettl5*^{1bp}, suggesting a role of rRNA methylation in these processes.

The ortholog of Mettl5 in humans is METTL5, mutation of which causes intellectual disability (ID) (*Richard et al., 2019*). This study expanded our understanding of the molecular mechanism of *Mettl5* function, which potentially provides new insights for the potential treatment of ID. Previous clinical studies found that the ID patients have sleep problems, including sleep duration shortness. This symptom is consistent with what we found for the *Mettl5*^{1bp}. The mechanism for this phenotype found in this study is potentially important. More studies need to be done in vertebrates to verify if this mechanism is conserved for sleep disorders.

The RNA-seq and Ribo-seq of *Mettl5*^{1bp} revealed the gene network that is potentially directed by *Mettl5*. The direct or immediate effect of *Mettl5* may lie in the regulation of translation. Indeed, we found that the codon occupancy was significantly changed for GAC, GAU, UCC. Moreover, the occupancy on dORF were significantly downregulated in the *Mettl5*^{1bp}. The translated uORF were significantly downregulated by the *Mettl5*^{1bp}. These may lead to fluctuations in certain protein production, which may eventually lead to altered downstream gene expression. This result indicated that small perturbations in translation process have a significant impact on downstream events,

highlighting the importance of maintaining the accuracy of the translation process.

We observed a significant decrease in total RNA and 18S rRNA methylation levels in individuals with the heterozygous allele of *Mettl5*. Interestingly, this finding differs slightly from studies conducted in mice, where heterozygous knockouts still exhibited normal levels of 18S rRNA m^6A methylation (*Sepich-Poore et al., 2022*). It may attribute to potential species-specific regulatory differences between *Drosophila* and mice. Another plausible explanation may lie in the distinct nature of the knockdown compared to knockouts. Notably, prior research has highlighted compensation effects arising from complete knockouts (*Teng et al., 2013; Rossi et al., 2015; Vu et al., 2015; Ma et al., 2019; El-Brolosy et al., 2019*).

This study revealed a new aspect on the connection of clock genes and proteasome. The clock regulation on proteasome was important in several different contexts. Previous studies showed that the circadian clock rhythmically controls the daily expression of multiple components of the proteasome, which responds to dietary restriction in *Drosophila* fat body (*Hwangbo et al., 2023*). In this study, we found *Mettl5* can regulate clock protein synthesis and degradation in clock neurons via affecting proteasome function. The role played by *Mettl5* in this process may be through affecting the methylation of ribosomes in clock neurons, affecting the proteasome degradation pathway (*Costa et al., 2019*), and ultimately leading to changes in clock proteins in clock neurons.

The function of Mettl5 highlights an integrative regulation of rRNA methylation and the proteasome. This provides an opportunity to coordinate protein synthesis and protein degradation, which would be a feasible way to keep balance for the total protein level. Interestingly, we observed specificity in the downstream affected genes both at transcriptional and translational levels. For the proteasome subunits, we also detected level changes for some of them, indicating a specificity of *Mettl5* function. The specificity for the proteasome subunits changes could be attributed to gene specificity of *Mettl5* on translation. Another possibility is that there are other layers of regulation on protein degradation pathway by Mettl5 protein interaction or other mechanisms. These factors may form a regulatory network to coordinate with each other. It is an intriguing question how the downstream specificity is achieved. More studies are needed to elucidate these mechanisms.

This result indicates the complex relationship between clock genes and sleep homeostasis regulation.

The data in this study are consistent with previous reports on the involvement of clock genes in the regulation of sleep homeostasis. It has been reported that loss of function alleles of *Per* and *Clock* exhibit a more pronounced sleep rebound after sleep deprivation (*Shaw et al., 2002*). Conversely, the *Mettl5* allele, which results in increased PER protein, leads to reduced sleep rebound. Furthermore, data in this study suggested that the regulatory mechanism of *Clock* has tissue specificity. According to the expression patterns of *Mettl5* based on *Mettl5*-Gal4, it does not express in clock neurons. Instead, it is expressed in *Mettl5*-Gal4 positive cells, which are composed of a part of neurons and glia. *Clock* is expressed not only in clock neurons of the *Drosophila* brain (*Patop et al., 2023*). The combinational expression of these proteins constitutes the specificity of clock upstream regulators. Our study indicates that these *Mettl5* expressing neurons and glia are important in sleep regulation. It would be interesting to find out the *Mettl5* dependent sleep homeostasis regulatory circuits.

Evidence indicates that sleep functions in development, metabolism and neuronal plasticity (*Anafi et al., 2019*). Sleep exerts effects on neuronal plasticity by modifying synapses. The synaptic homeostasis theory proposes that sleep has a role in downscale synaptic strength (*Tononi and Cirelli, 2006*). Indeed, synapse markers progressively decrease during sleep in both mammals and *Drosophila* brains (*López-Varea et al., 2021; Vyazovskiy et al., 2008; Gilestro et al., 2009; Liu et al., 2010*) More importantly, evidence indicates that sleep need and protein levels in synapse are tightly linked. Studies of the presynaptic active zone have shown that synaptic plasticity regulates sleep homeostasis (*Huang et al., 2020*). Genome-wide proteomic studies of synapse in mouse brain indicate that the synaptic proteins peak around dusk and dawn (*Noya et al., 2019; Brüning et al., 2019*). Sleep deprivation experiments have demonstrated that the sleep drive is significantly dependent on the cycling of proteins and phosphoproteins in synapses, in contrast to mRNAs (*Noya et al., 2019; Brüning et al., 2019*). These results suggest that the gene expression regulation at the protein level is crucial for sleep. Consistently, we detected changes in the quantity of axons in *Mettl5*^{1bp}, suggesting a possible regulation of neural circuits by *Mettl5*.

This study revealed gene-specific functions of ribosome components. Previous study suggested a context dependent component and function of ribosomes (*Simsek et al., 2017*). We observed changes in the translational efficiency of genes in the *Mettl5* mutant. One possible mechanism is that rRNA

337 modifications influenced by *Mettl5* affect the binding affinity of ribosomes to specific RNA sequences.
338 Alternatively, the rRNA modifications influenced by *Mettl5* may be responsible for certain ribosome
339 types that impact the translation of this gene profile. Further evidence is needed to elucidate these
340 possibilities.

341 **Material and methods**

342 **Drosophila Strains**

343 Fly stocks used in this study were maintained under standard culture conditions. We used the w^{1118} as
344 the control strain. The following flies were obtained from Bloomington Stock Center: w^{1118} (Bl: 5905),
345 *Mettl5*-Gal4 (Bl: 19514), *Repo*-Gal4 (Bl: 7415), *nSyb*-Gal4 (Bl: 51941), *pdf*-Gal4 (Bl: 41286), Clk^{JRK}
346 (Bl: 80927), per^{01}(Bl: 80917), $Fmr1^{\Delta 50M}$(Bl: 6930)，UAS-*Trmt112*RNAi (VDRC: 101515), UAS-
347 DenMark,UAS-*syt*.eGFP (Bl: 33064), UAS-GFPstinger (from Yi Rao's lab), UAS-*Fmr1* (Bl: 6931),
348 UAS-*Mettl5* (FlyORF: F000760) are from Fly ORF collection. UAS-*Mettl5m*-3HA (generated in this
349 study). $Mettl5^{1bp}$ and $Mettl5^{9bp}$ were generated by the CRISPR/Cas system.

350 **Sleep behavior assays**

351 Sleep assays were performed in an incubator at a temperature of 25 ± 1 °C and a relative humidity
352 of 60% ± 5%. Lights were turned on at ZT0 (06:30 am) and off at ZT12 (18:30 pm). The locomotor
353 activity was recorded using Drosophila Activity Monitoring System (Trikinetics. Waltham,
354 MA). Flies were acclimated to the experimental conditions for 2 days before data collection.
355 Locomotor activity data were collected at 1-minute intervals for 3 days, and analyzed by pysolo as
356 described previously (*Gilestro and Cirelli, 2009*). Sleep was defined as periods of 5 min or more of
357 behavioral immobility.

358 Sleep deprivation is applied by mechanical stimuli using a timer-controlled rotating shaker. The
359 intensity of stimuli was 1500 rpm once every minute (2 s/1 min) (*Shimizu et al., 2008*). After
360 acclimating to the experimental conditions for 2 days, the flies were sleep deprived for 12 h (ZT12-
361 ZT24). Mechanical sleep deprivation was performed using the SNAP method to keep flies awake for
362 12 h overnight (*Shaw et al., 2002*). Flies were sleep deprived from ZT12 (beginning of the dark phase)
363 to ZT0 (beginning of the light phase) by a vortex at the lower intensity setting for 3 s every minute.
364 Sleep lost and recovery were calculated for each fly by using the 24-h period preceding deprivation as

365 the baseline. Sleep recovery values were calculated by subtracting 6 h sleep amount during night
366 (ZT12-ZT18) after deprivation from the sleep amount of the corresponding time of the previous day
367 (baseline sleep amount).

368 Sleep arousal is measured at ZT14. Flies are given a uniform, gentle mechanical stimulus, and
369 any activity within the next five minutes is recorded. If no activity is observed during this period, the
370 fly is considered not to have awakened in response to the stimulation. The number of flies that awaken
371 due to the stimulus is counted, and their percentage is calculated.

372 **Statistical analysis**

373 Statistical analysis was carried out in GraphPad Prism 5. The statistical tests for each experiment are
374 shown in the figures. The significance of difference for sleep parameters was analyzed using
375 Nonparametric test, including two-tailed Mann-Whitney test or one-way ANOVA with Tukey's
376 multiple comparison test. Unpaired Student's t-test analyses were carried out for qPCR data and Log-
377 rank (Mantel-Cox) test analyses were carried out for lifespan data using GraphPad Prism software.
378 For all statistical tests, $p < 0.05$ was considered significant.

379 **Quantitative PCR**

380 Total RNA was extracted from cells and tissues using the TRNzol Universal Reagent (Tiangen #DP4-
381 02). RNA reverse transcription was performed by using PrimeScript RT reagent Kit with gDNA Eraser
382 (TAKARA #RR047A). Quantitative PCR was carried out using SuperReal PreMix Plus (SYBR Green)
383 (Tiangen #DP4-02). *RP49* were used to normalize results between groups. Three independent
384 biological replicates were performed for each experiment. The primers used in this experiment are
385 *RP49*-F: CGGTTACGGATCGAACAAGC; *RP49*-R: CTTGCGCTTCTTGGAGGAGA; *Mettl5*-F:
386 CAACACGGTCGTACATTCAG; *Mettl5*-R: AGTCCACCTC AATATCCTTCG.

387 **Imaging and analysis of axon volume**

388 To quantify the axon volume of small LNvs, the plugin Object 3D counter in ImageJ was used to
389 quantify number of pixels from the raw images. The images were processed according to a threshold
390 in which an intact axon can be observed in controls. Axon span from the first axonal bifurcation to the
391 tip of the terminal which was labeled by white rectangular box in Figure 8 was quantified.

392 **Sample collection and library construction for Ribo-seq and RNAseq**

For *Drosophila* samples, the w^{1118} and $Mettl5^{1bp}$ at ZT15 were transferred to centrifuge tubes and quick-frozen by immersion in liquid nitrogen. The fly heads were separated and collected after quick-frozen with liquid nitrogen. Three biological replicates were collected for w^{1118} and $Mettl5^{1bp}$, respectively. Half of each sample was used for RNA-seq and the other half for Ribo-seq.

For Ribo-seq library construction, samples were treated with specific lysis buffer with cycloheximide (50mg/mL) to acquire the lysate (Novogen, China). To digest the RNA other than ribosome-protected fragments (RPF), fly tissue lysate was treated with unspecific endoribonuclease, RNase I. Isolation of monosomes was performed by size-exclusion chromatography using MicroSpin S-400 HR columns. The RNA samples were then treated with rRNA depletion kit to remove as much rRNA contamination as possible before performing PAGE purification of the relatively short (20~38 nt) RPFs. Following PAGE purification, both ends of the RPF were phosphorylated and ligated with 5' and 3' adapters, respectively. Then the fragments were reversely transcribed to the cDNAs, amplified by PCR, and subjected to library construction after quality test. Ribo-seq libraries were sequenced using PE150 (Illumina).

For RNA-seq library construction, total RNA was extracted using a standard TRIzol RNA extraction protocol. The cDNA library was built and sequenced using illumina PE 150 (Illumina). The RNAseq analysis was performed by Novogen.

Ribo-seq and RNA-seq data were analyzed as follows. Raw data (raw reads) of FASTQ format were first processed. Clean reads were obtained by removing reads containing adapters, reads containing N bases and low-quality reads from the raw data. At the same time, Q20, Q30 and GC content of the clean data were calculated.

RNA-seq analysis

Index of the *Drosophila melanogaster* reference genome (dm6) was built using Hisat2 v2.0.5 (*Kim et al., 2019*) and paired-end clean reads were aligned to the *Drosophila melanogaster* reference genome (dm6) using Hisat2 v2.0.5. The mapped reads of each sample were assembled by StringTie (v1.3.3b) (*Pertea et al., 2015*) in a reference-based approach. FeatureCounts (v1.5.0) (*Liao et al., 2014*) was used to count the reads numbers mapped to each gene. Differential expression analysis of w^{1118} and $Mettl5^{1bp}$ was performed using the DESeq2 R package (1.20.0) (*Pertea et al., 2015*). Genes with

421 an adjusted P-value<0.05 and |log2fc| ≥1 were assigned as significant differentially expressed gene.

422 **Ribo-seq analysis**

423 First, the clean reads were aligned to a FASTA file containing rRNA, tRNA, snoRNA, and snRNA
424 from Flybase Release 6.13 annotations using Bowtie (*Liao et al., 2014*) with a maximum of two
425 mismatches (-v 2) by default. Successful alignments were discarded, and all unaligned reads were
426 collected. Unaligned clean reads (ribosome-protected fragments, RPF) were then mapped to the
427 FlyBase D. melanogaster reference genome (Release 6.13) using STAR (v2.7.3a) (*Dobin et al., 2013*)
428 with default options. The unique genome-mapped reads are then mapped against protein coding
429 transcripts using Bowtie (v1.2.2) (*Langmead et al., 2009*) with parameters "-a -v 2" by default. The
430 featureCounts program in Subread package v1.6.3 is used to count the number of RPFS uniquely
431 mapped to CDS regions based on fly genome mapping file (-t CDS -g gene_id), which were then
432 normalized as RPF Per Kilobase per Million mapped RPFs (RPKM). DESeq2 R package (1.14.1)
433 (*Love et al., 2014*) was used for differential expression analysis. The threshold for significantly
434 differential expression is $|\log_2 (\text{Fold Change})| \geq 0.265$ & $p^{adj} < 0.05$. Differential TE analysis was
435 performed using RiboDiff. Coding frame distribution and 3-nt periodicity analyses for Ribo-seq
436 quality evaluation were performed using R package riboWaltz (v1.1.0) (*Lauria et al., 2018*). The
437 Ribocode package (*Xiao et al., 2018*) was used to analyze the P-site and the motif of
438 translated/untranslated uORFs. Gene Ontology (GO) and KEGG pathway analysis, Gene Set
439 Enrichment Analysis (GSEA) analysis was performed using the clusterProfiler package (v4.5.2.002)
440 (*Wu et al., 2021*). Volcano plots, veen plots a were plotted with the ggplot2 package.
441 SimplifyEnrichment package (*Gu and Hübschmann, 2022*) was used to simply the GO enrichment
442 results.

443 **Immunofluorescence experiments**

444 Adult flies that were 7-15 days old (unless otherwise noted) were anaesthetized with CO_2 and dissected
445 in 0.03% PBST (1 × PBS with 0.03% Triton X-100; Sigma, T9284) on ice. After a 55 min fixation of
446 samples in 2% paraformaldehyde (PFA) at room temperature (RT), samples were washed four times
447 for 15 min in 0.03% PBST at RT, blocked in 10% Normal Goat Serum (NGS; diluted with 1 × PBS
448 with 2% Triton) overnight at 4°C and incubated with primary antibodies for 24 h at 4°C. The samples

449 were washed again four times with 1 × PBS with 1% Triton for 15 min at RT and incubated with
450 secondary antibodies overnight at 4 °C. And then the samples were washed with 1 × PBS with 1%
451 Triton again 4 times for 15 min at RT and mounted on a slide using anti-fading Mounting medium
452 (with DAPI; Solarbio, S2110). The primary antibodies we used were anti-Elav rat (DSHB, 7E8A10,
453 1:200) and anti-Repo mouse (Developmental Studies Hybridoma Bank, 8D12; 1:200). The secondary
454 antibodies were Alexa FluorTM 568 (Thermo Fisher Scientific, A11004; 1:200) and Alexa FluorTM
455 647 (Thermo Fisher Scientific, A21247; 1:200). The primary and secondary antibodies were diluted
456 in dilution buffer (1.25% PBST, 1% NGS). Images were taken using confocal microscopy (Leica SP8)
457 with LAX software with auto Z brightness correction to generate a homogeneous signal where it
458 seemed necessary and were formatted using Adobe Photoshop CS6. Figures were generated using
459 Adobe IIIustrator 2020. For the immunofluorescence experiment of PDF, the method is similar with
460 the discription above. All immunofluorescence experiments were done with at least 3 repeats, each
461 repeat with a sample size of more than 10 individual flies. ImageJ was used to analyze
462 immunofluorescence brightness.

463 **Western Blotting**

464 Total protein was extracted from approximately 30 fly heads using RIPA buffer (150 mM NaCl,
465 1.0% NP-40, 0.5% sodium deoxycholate, 0.1% SDS, 50 mM Tris-HCl, pH 8.0). Protease inhibitor
466 cocktail (CW2200S) and phosphatase inhibitor cocktail (CW2383S) were added according to the
467 manufacturer's instructions. An equal volume of 2x SDS loading buffer was added to the samples,
468 followed by heating in a water bath at 100 °C for 5 minutes, and then cooling on ice for several minutes.

469 Primary antibodies (Rabbit anti-PER, Gift from Dr. Jeffrey Price's laboratory at University of
470 Missouri at Kansas City, U.S.) were diluted 1:5000 and incubated with the membranes overnight at
471 4°C, while HRP-labeled secondary antibodies (HRP Goat Anti-Rabbit IgG (H + L) (ABclonal, AS014))
472 were diluted 1:1500 and incubated for 4 hours at room temperature. Signals were detected using ECL
473 (ABclonal, RM00021P) and visualized with the Amersham ImageQuant 800 (GE Healthcare, Sweden).
474 Signal intensity was quantified using ImageJ software. Three biological replicates were conducted for
475 this experiment.

476 **LC-MS/MS analysis of m^6A levels**

Total RNA was extracted from cells and tissues using TRNzol Universal Reagent (Tiangen #DP4-02). 18S rRNA was obtained through polyacrylamide gel electrophoresis and gel recovery of total RNA. Ribonucleoside standards included rA and N6 mA. The fluid phase used in this experiment was a mixture of methanol and ddH_2O. For each biological replicate, 1 μg of total RNA or 18S rRNA was degraded to single nucleotides using Nucleoside Digestion Mix (NEB #M0649), followed by the addition of a 4-fold volume of methanol and precipitation at -20°C for 2 hours to remove proteins. Multiple reaction monitoring transitions used in this study were 268.10275→136.0621 (rA), 282.11835→150.0774 (N6 mA).

Lifespan and Negtive geotaxis RING assay

Mated males were collected and maintained at a density of 20 flies per vial. The flies were kept at a temperature of 25 °C with 60% humidity and a 12-hour light/12-hour dark cycle. Every other day, the flies were transferred to new vials, and their survival rate was recorded. Statistical analysis and survival curve plotting were performed using GraphPad Prism 5.0. Each experiment was conducted with three biological replicates, using a total of 300 flies for lifespan assays.

For climbing assays, flies were collected under CO_2 anesthesia and allowed to recover overnight. Typically, 200 flies (distributed among 10 vials, each containing 20 flies and marked at 90 mm from the bottom) were used for each genotype. To initiate the climbing assay, vials were tapped sharply on the table three times to elicit negative geotaxis responses. A 15-minute rest period was observed between each trial. Three trials were conducted for each group, and five groups were used for each genotype. The number of flies attempting to reach the mark within 10 seconds was counted for each trial. Videos were recorded during the assay, and the positions of the flies were captured. The camera and vials were separated by a 20 cm distance, and a white open-faced box placed behind the setup provided uniform lighting.

Data availability

The RNA-seq and Ribo-seq data from this publication have been deposited to the NCBI bioproject database https://www.ncbi.nlm.nih.gov/bioproject/ and assigned the identifier PRJNA994860.

Acknowledgements

This work was supported by National Natural Science Foundation of China (Grant No. 32070492 and 32122017) to Juan Du.

Author contributions

XW and TF designed and performed the experiments, analyzed the data and wrote the manuscript. XY performed the bioinformatics analysis, analyzed the data and edited the manuscript. YR analyzed data and edited the manuscript. JD designed experiments, analyzed data, wrote and edited the manuscript. All authors have read and approved the final manuscript.

Declaration of interest

The authors declare that they have no conflict of interest.

Supplementary information

Supplementary Figures S1-S11

Supplementary Table1

Figure legends

Figure 1 *Mettl5* is a regulator of *Drosophila* sleep.

(A) Diagram illustrating CRISPR-Cas knockout of 1 or 9 bases in the *Mettl5* gene. (B) Relative expression of *Mettl5* mRNA in *Mettl5*^{1bp} and *Mettl5*^{9bp} mutant male flies compared to control flies. (C) Sleep curve throughout the day for *Mettl5* mutant male flies and control flies. (D) Total sleep of *Mettl5* mutant male flies and control flies. (E) Sleep bout duration of *Mettl5* mutant male flies and control flies. (F) Number of sleep bouts of *Mettl5* mutant male flies and control flies. (G) Percentage of awake for *Mettl5* mutant flies and control flies. (H) Sleep curve throughout the day for *Mettl5* mutant male flies, induced *Mettl5* over expression male flies and control flies. (I) Total sleep of *Mettl5* mutant male flies, induced *Mettl5* over expression male flies and control flies. (J) Sleep bout duration of *Mettl5* mutant male flies, induced *Mettl5* over expression male flies and control flies. (K) Number of sleep bouts of *Mettl5* mutant male flies, induced *Mettl5* over expression male flies and control flies. (L) Percentage of awake for *Mettl5* mutant flies, *Mettl5* over expression male flies and control flies. (M)

530 Sleep curve is tracked throughout the entire day prior to sleep deprivation and during the daytime sleep
531 rebound period. (N) *Mettl5* mRNA expression level at different time points. W(wake), SD (sleep
532 deprivation), SR (sleep recovery). (O) The daytime sleep recovery during the six hours following sleep
533 deprivation in *Mettl5* mutant male flies. For * stands for p<0.05, ** stands for p<0.01, *** stands for
534 p<0.001, *ns* stands for not significant.

535 **Figure 2 *Mettl5* regulation of *Drosophila* sleep was dependent on its methyltransferase activity.**
536 (A) The m^6A level in the total RNA of *Mettl5* mutant male flies. (B) The m^6A level in the 18S rRNA
537 of *Mettl5* mutant male flies. (C) The sleep curve throughout the day shows the sleep pattern of induced
538 *Trmt112* RNAi male flies and control flies. (D) Total sleep of induced *Trmt112* RNAi male flies and
539 control flies. (E) Sleep bout duration in induced *Trmt112* RNAi male flies and control flies. (F)
540 Number of sleep bouts in induced *Trmt112* RNAi male flies and control flies. (G) Percentage of awake
541 in *Trmt112* RNAi and control flies. (H) Sleep curve throughout the day for *Mettl5* mutant male flies,
542 induced *Mettl5m* over expression male flies and control flies. (I) Total sleep of *Mettl5* mutant male
543 flies, induced *Mettl5m* over expression male flies and control flies. (J) Sleep bout duration in *Mettl5*
544 mutant male flies, induced *Mettl5* over expression male flies and control flies. (K) Number of sleep
545 bouts in *Mettl5* mutant male flies, induced *Mettl5* over expression male flies and control flies. (L)
546 Percentage of awake in *Mettl5* mutant male flies, induced *Mettl5* over expression male flies and control
547 flies. For * stands for p<0.05, ** stands for p<0.01, *** stands for p<0.001, *ns* stands for not significant.

548 **Figure 3 RNA-seq and Ribo-seq analysis revealed changes in the gene profile of *Mettl5*^{1bp}.**
549 (A) Venn diagram depicting the number of significant differentially expressed genes revealed by RNA-
550 seq and Ribo-seq. (B) Volcano plot representing the differentially expressed genes identified by RNA-
551 seq. Genes that met the criteria of |log2(fold-change)| ≥ 1 and p.adjust < 0.05 were considered
552 significantly expressed, marked in orange for downregulation and green for upregulation. (C) Volcano
553 plot representing the differentially expressed genes identified by Ribo-seq. Candidates that satisfied
554 the criteria of $|\log_2(\text{fold-change})| \geq 0.265$ and p.adjust <0.05 were regarded as significantly expressed,
555 marked in red for downregulation and blue for upregulation, respectively. (D-K) Gene set enrichment
556 analysis of differentially expressed genes revealed by RNA-seq (D-G) and Ribo-seq (H-K). All the
557 plots are generated using the KEGG gene set database. The bar chart at the bottom of each panel shows

558 the distribution of target genes for each pathway according to their rank position. Each vertical line
559 represents a gene. Genes on the left show positive correlation with *Mettl5*^{1bp}, while, genes on the right
560 show negative correlation with *Mettl5*^{1bp}. The green line indicates the enrichment score (ES), and NES
561 stands for normalized enrichment score. (L) Distribution of the differentially expressed genes revealed
562 by both RNA-seq and Ribo-seq. (M) Cumulative distribution of TE frequencies among w^{1118} and
563 *Mettl5*^{1bp} (N, O) GO and KEGG enrichment of significantly changed TE-related genes between w^{1118}
564 and *Mettl5*^{1bp}. The color of the bar indicates the enrichment p.adjust value. (P) KEGG network
565 showing the top 5 pathway and associated genes. The size of the dots represents the number of genes
566 in the pathway.

567 **Figure 4. Clock genes expression mediated the sleep phenotype caused by *Mettl5* mutation.**

568 (A-C) Fold changes in clock genes with significant expression level differences between w^{1118} and
569 *Mettl5*^{1bp} were observed in RNA-seq, Ribo-seq, and translation efficiency analyses. (D-E) PER protein
570 immunofluorescence staining in small LNvs (ventral lateral neurons) and its immunofluorescence
571 intensity statistics. (F-G) Western blot analysis of PER protein and Tubulin protein, along with their
572 grayscale quantification. (H) Sleep curves throughout the day for *Mettl5*^{1bp}, *CLK*^{JRK}, double mutant
573 and control flies. (I) Total sleep for *Mettl5*^{1bp}, *CLK*^{JRK}, double mutant and control flies. (J) Percentage
574 of awake time in *Mettl5*^{1bp} flies, partially rescued by double mutant flies. (K) Sleep curve throughout
575 the day for *Mettl5*^{1bp}, *per*^{01}, double mutant and control flies. (L) Total sleep for *Mettl5*^{1bp}, *per*^{01}, double
576 mutant and control flies. (M) Percentage of awake time in *Mettl5*^{1bp} flies, partially rescued by double
577 mutant flies. (N) Fold changes in proteasome subunits with significant expression level differences
578 between w^{1118} and *Mettl5*^{1bp} were observed in RNA-seq, Ribo-seq, and translation efficiency analyses.
579 For statistical significance, * stands for $p<0.05$, ** stands for $p<0.01$, *** stands for $p<0.001$, *ns* stands
580 for not significant.

581 Figure 5 A working model illustrating the role of *Mettl5* in *Drosophila* sleep was presented.

582 **Figure 6 The axon complexity was found to be affected by *Mettl5*^{1bp}**

583 (A-D) Examples of small LNvs axonal terminals labeled by syt-eGFP (green). A rectangular box
584 indicates the location where LNvs axons exit the posterior optic tract and the first axonal bifurcation
585 to the tip of the terminal region, whose volume was measured. (E) Mean volume measurements of

586 small LNvs axonal terminals labeled by syt-eGFP.

587 **Table 1 Circadian rhythm phenotypes of various mutants.**

588

589 **References**

590 Anafi RC, Kayser MS, Raizen DM. 2019. Exploring phylogeny to find the function of sleep. *Nature*
591 *Reviews Neuroscience* 20: 109-116.

592 Brüning F, Noya SB, Bange T, Koutsouli S, Rudolph JD, Tyagarajan SK, Cox J, Mann M, Brown SA,
593 and Robles MS. 2019. Sleep-wake cycles drive daily dynamics of synaptic
594 phosphorylation. *Science* 366: eaav3617.

595 Bushey D, Tononi G, Cirelli C. 2011. Sleep and synaptic homeostasis: structural evidence in *Drosophila*.
596 *Science* 332: 1576-1581.

597 Costa RO, Martins H, Martins LF, Cwetsch AW, Mele M, Pedro JR, Tomé D, Jeon NL, Cancedda L,
598 Jaffrey SR, Almeida RD. 2019. Synaptogenesis Stimulates a Proteasome-Mediated Ribosome
599 Reduction in Axons. *Cell Reports* 28: 864-876.

600 Desvergne A, Ugarte N, Radjei S, Gareil M, Petropoulos I, Friguet B. 2016. Circadian modulation of
601 proteasome activity and accumulation of oxidized protein in human embryonic kidney HEK 293 cells
602 and primary dermal fibroblasts. *Free Radical Biology And Medicine* 94: 195-207.

603 Dobin A, Davis CA, Schlesinger F, Drenkow J, Zaleski C, Jha S, Batut P, Chaisson M, Gingeras, TR.
604 2013. STAR: ultrafast universal RNA-seq aligner. *Bioinformatics* 29: 15-21.

605 Du J, Lv P, Fu T, Wei Y, Zhao Z. 2021. Regulation of sleep in *Drosophila melanogaster*. Adv *Insect*
606 *Physiol* 60: 119-168.

607 El-Brolosy MA, Kontarakis Z, Rossi A, Kuenne C, Gunther S, Fukuda N, Kikhi K, Boezio GLM, Takacs
608 CM, Lai SL. 2019. Genetic compensation triggered by mutant mRNA degradation. *Nature* 568: 193-
609 197.

610 Fernández-Cruz I, Sánchez-Díaz I, Narváez-Padilla V, Reynaud E. 2020. Rpt2 proteasome subunit
611 reduction causes Parkinson's disease like symptoms in *Drosophila*. *IBRO Reports* 9: 65-77.

612 Galimberti V, Kinor N, Shav-Tal Y, Biggiogera M, Brüning A. 2016. The stress-inducible transcription
613 factor ATF4 accumulates at specific rRNA-processing nucleolar regions after proteasome inhibition.

European Journal of Cell Biolog 95: 389-400.

Gilestro GF, Tononi G, Cirelli C. 2009. Widespread changes in synaptic markers as a function of sleep and wakefulness in *Drosophila*. *Science* 324: 109-112.

Gilestro GF, Cirelli C. 2009. pySolo: a complete suite for sleep analysis in Drosophila. *Bioinformatics* 25: 1466-1467.

Gu Z, Hübschmann D. 2022. simplifyEnrichment: A bioconductor package for clustering and visualizing functional enrichment results. *Genomics Proteomics Bioinformatics* 21: 190-202.

Huang S, Piao C, Beuschel CB, Götz T, Sigrist SJ. 2020. Presynaptic active zone plasticity encodes sleep need in Drosophila. *Current Biology* 30: 1077-1091.

Hwangbo DS, Kwon YJ, Iwanaszko M, Jiang P, Abbasi L, Wright N, Alli S, Hutchison AL, Dinner AR, Braun RI, Allada R. 2023. Dietary Restriction Impacts Peripheral Circadian Clock Output Important for Longevity in *Drosophila*. bioRxiv [Preprint]. 2023.01.04.522718. DOI: 10.1101/2023.01.04.522718. PMID: 36711760

Kapetanou M, Athanasopoulou S, Gonos ES. 2022. Transcriptional regulatory networks of the proteasome in mammalian systems. *IUBMB Life* 74: 41-52.

Kim D, Paggi JM, Park C, Bennett C, Salzberg SL. 2019. Graph-based genome alignment and genotyping with HISAT2 and HISAT-genotype. *Nature Biotechnology* 37: 907-915.

Langmead B, Trapnell C, Pop M, Salzberg SL. 2009. Ultrafast and memory-efficient alignment of short DNA sequences to the human genome. *Genome Biology* 10: R25.

Lauria F, Tebaldi T, Bernabò P, Groen EJN, Gillingwater TH, Viero G. 2018. riboWaltz: Optimization of ribosome P-site positioning in ribosome profiling data. *PLoS Computational Biology* 14: e1006169.

Leismann J, Spagnuolo M, Pradhan M, Wacheul L, Vu MA, Musheev M, Mier P, Andrade-Navarro MA, Graille M, Niehrs C, Lafontaine DL, Roignant JY. 2020. The 18S ribosomal RNA m^6A methyltransferase *Mettl5* is required for normal walking behavior in *Drosophila*. *EMBO Reports* 21: e49443.

Liao Y, Smyth GK, Shi W. 2014. featureCounts: an efficient general purpose program for assigning sequence reads to genomic features. *Bioinformatics* 30: 923-930.

Liu ZW, Faraguna U, Cirelli C, Tononi G, Gao XB. 2010. Direct evidence for wake-related increases

642 and sleep-related decreases in synaptic strength in rodent cortex. *Journal Of Neuroscience* 30: 8671-
643 8675.
644 López-Varea A, Vega-Cuesta P, Ruiz-Gómez A, Ostalé CM, Molnar C, Hevia CF, Martín M, Organista
645 MF, de Celis J, Culí J, Esteban N, de Celis JF. 2021. Genome-wide phenotypic RNAi screen in the
646 Drosophila wing: phenotypic description of functional classes. G3 (Bethesda). *11*, jkab349. DOI:
647 10.1093/g3journal/jkab349. PMID: 34599810
648 Love MI, Huber W, Anders S. 2014. Moderated estimation of fold change and dispersion for RNA-seq
649 data with DESeq2. *Genome Biology* 15: 550.
650 Lyons LC, Vanrobaeys Y, Abel T. 2023. Sleep and memory: The impact of sleep deprivation on
651 transcription, translational control, and protein synthesis in the brain. *Journal Of Neurochemistry*
652 166: 24-46.
653 Ma Z, Zhu P, Shi H, Guo L, Zhang Q, Chen Y, Chen S, Zhang Z, Peng J, Chen J. 2019. PTC-bearing
654 mRNA elicits a genetic compensation response via Upf3a and COMPASS components. *Nature* 568:
655 259-263.
656 Noya SB, Colameo D, Brüning F, Spinnler A, Mircsof D, Opitz L, Mann M, Tyagarajan SK, Robles MS,
657 Brown SA. 2019. The forebrain synaptic transcriptome is organized by clocks but its proteome is
658 driven by sleep. *Science* 366: eaav2642.
659 Palanca A, Casafont I, Berciano MT, Lafarga M. 2014. Reactive nucleolar and Cajal body responses to
660 proteasome inhibition in sensory ganglion neurons. *Biochimica et Biophysica Act* 1842: 848-859.
661 Patop IL, Anduaga AM, Bussi IL, Ceriani MF, Kadener S. 2023. Organismal landscape of clock cells
662 and circadian gene expression in *Drosophila*. bioRxiv [Preprint]. 2023.05.23.542009.
663 Pertea M, Pertea GM, Antonescu CM, Chang TC, Mendell JT, Salzberg SL. 2015. StringTie enables
664 improved reconstruction of a transcriptome from RNA-seq reads. *Nature Biotechnology* 33: 290-295.
665 Philpott JM, Freeberg AM, Park J, Lee K, Ricci CG, Hunt SR, Narasimamurthy R, Segal DH, Robles
666 R, Cai Y, Tripathi S, McCammon JA, Virshup DM, Chiu JC, Lee C, Partch CL. 2023. PERIOD
667 phosphorylation leads to feedback inhibition of CK1 activity to control circadian period. *Molecular*
668 *Cell* 83: 1677-1692.
669 Richard EM, Polla DL, Assir MZ, Contreras M, Shahzad M, Khan AA, Razzaq A, Akram J, Tarar MN,

Blanpied TA, Ahmed ZM, Abou Jamra R, Wieczorek D, van Bokhoven H, Riazuddin S, Riazuddin S. 2019. Bi-allelic variants in METTL5 cause autosomal-recessive intellectual disability and microcephaly. *American Journal Of Human Genetics* 105: 869-878.

Rossi A, Kontarakis Z, Gerri C, Nolte H, Holper S, Kruger M, Stainier DY. 2015. Genetic compensation induced by deleterious mutations but not gene knockdowns. *Nature* 524: 230-233

Sepich-Poore C, Zheng Z, Schmitt E, Wen K, Zhang ZS, Cui XL, Dai Q, Zhu AC, Zhang L, Sanchez Castillo A, Tan H, Peng J, Zhuang X, He C, Nachtergaele S. 2022. The METTL5-TRMT112 N6-methyladenosine methyltransferase complex regulates mRNA translation via 18S rRNA methylation. *Journal Of Biological Chemistry* 298: 101590.

Shaw PJ, Tononi G, Greenspan RJ, Robinson DF. 2002. Stress response genes protect against lethal effects of sleep deprivation in *Drosophila*. *Nature* 417: 287-291.

Shimizu H, Shimoda M, Yamaguchi T, Seong KH, Okamura T, Ishii S. 2008. *Drosophila* ATF-2 regulates sleep and locomotor activity in pacemaker neurons. *Molecular And Cellular Biology* 28: 6278-6289.

Simsek D, Tiu GC, Flynn RA, Byeon GW, Leppek K, Xu AF, Chang HY, Barna M. 2017. The Mammalian Ribo-interactome Reveals Ribosome Functional Diversity and Heterogeneity. *Cell* 169: 1051-1065.e18.

Teng X, Dayhoff-Brannigan M, Cheng WC, Gilbert CE, Sing CN, Diny NL, Wheelan SJ, Dunham MJ, Boeke JD, Pineda FJ. 2013. Genome-wide consequences of deleting any single gene. *Molecular Cell* 52: 485-494.

Tononi G, Cirelli C. 2006. Sleep function and synaptic homeostasis. *Sleep Medicine Reviews* 10: 49-62.

van Tran N, Ernst FGM, Hawley BR, Zorbas C, Ulryck N, Hackert P, Bohnsack KE, Bohnsack MT, Jaffrey SR, Graille M, Lafontaine DLJ. 2019. The human 18S rRNA m^6A methyltransferase METTL5 is stabilized by TRMT112. *Nucleic Acids Research* 47: 7719-7733.

Vu V, Verster AJ, Schertzberg M, Chuluunbaatar T, Spensley M, Pajkic D, Hart GT, Moffat J, Fraser AG. 2015. Natural variation in gene expression modulates the severity of mutant phenotypes. *Cell* 162: 391-402

Vyazovskiy VV, Cirelli C, Pfister-Genskow M, Faraguna U, Tononi G. 2008. Molecular and

electrophysiological evidence for net synaptic potentiation in wake and depression in sleep. *Nature Neuroscience* 11: 200-208.

Xiao Z, Huang R, Xing X, Chen Y, Deng H, Yang X. 2018. De novo annotation and characterization of the translatome with ribosome profiling data. *Nucleic Acids Research* 46: e61.

Wang L, Liang Y, Lin R, Xiong Q, Yu P, Ma J, Cheng M, Han H, Wang X, Wang G, Liang F, Pei Z, Chen D, Yuan Q, Jiang YZ, Lin S. Mettl5 mediated 18S rRNA N6-methyladenosine (m^6A) modification controls stem cell fate determination and neural function. 2020. *Genes & Diseases* 9: 268-274.

Wu T, Hu E, Xu S, Chen M, Guo P, Dai Z, Feng T, Zhou L, Tang W, Zhan L, Fu X, Liu S, Bo X, Yu G. 2021. clusterProfiler 4.0: A universal enrichment tool for interpreting omics data. *Innovation* (Camb) 2: 100141.

Genotype	NumTotal	%Rhythmic	Period	Power
w^{1118}	32	92.6	23.9± 0.05	127.9± 7.62
Mettl5 ^{1bp}/+	32	92.3	28.3± 0.4 ***	114.3± 6.76 ns
Mettl5 ^{1bp}/+ ; UAS-*Mettl5/Mettl5*Gal4	32	96.9	24± 0.02 ns	127.1± 5.42 ns
Mettl5 ^{1bp}/Clk^{JRK}	44	29.5	24± 0.04 ns	68.5± 8.85 ***
Mettl5 ^{1bp}/Per^{01}	54	9.3	24.2± 0.2 ns	43.8± 13.41 ***

Figure 1

Mettl5 allele verification

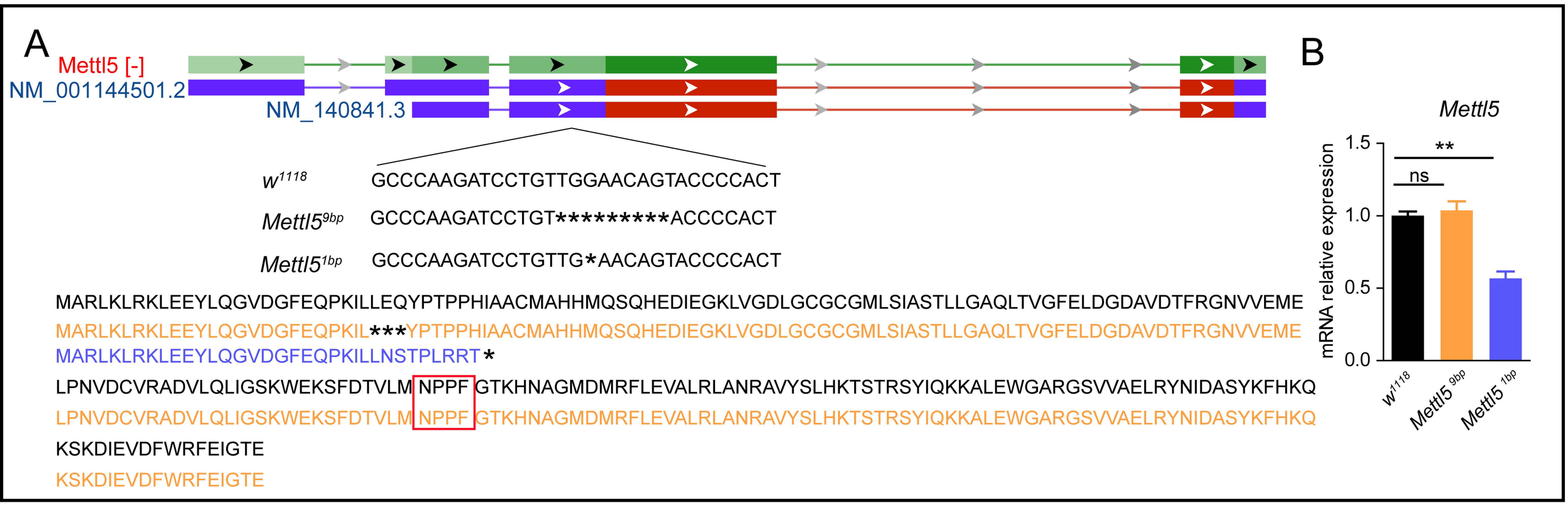

Sleep phenotypes

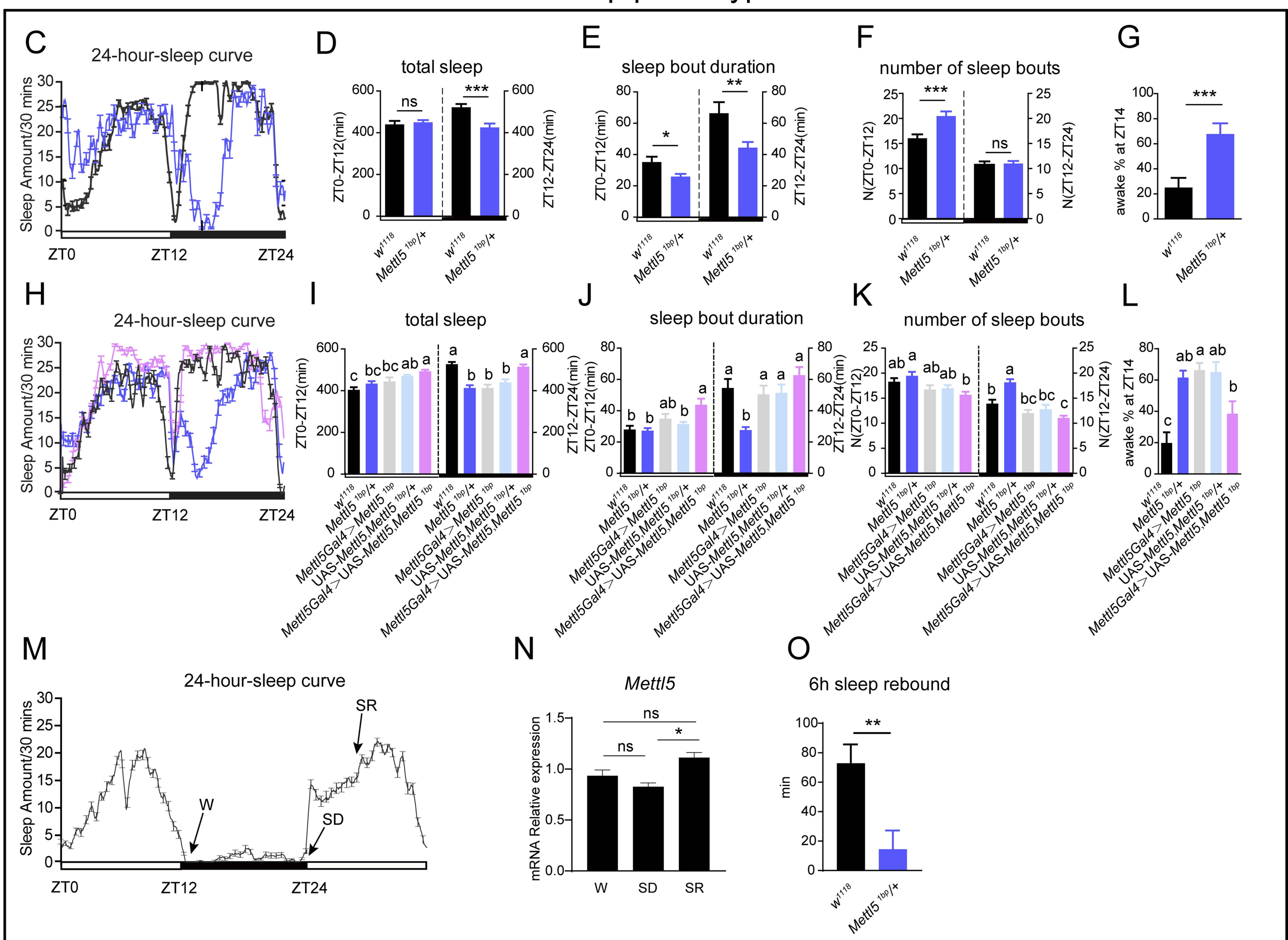

Figure 2

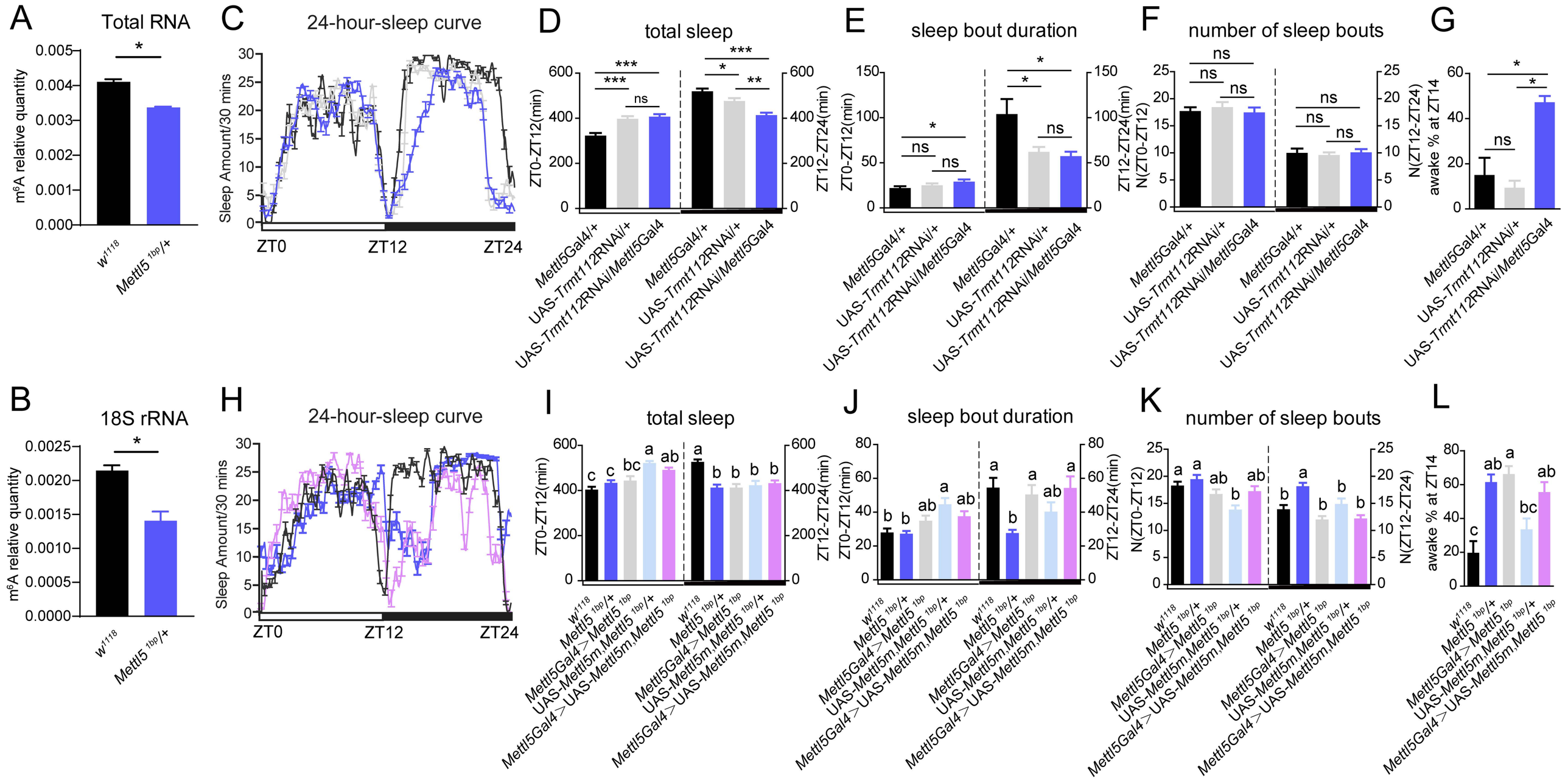
A
Total RNA
m6A relative quantity
0.005
0.004
0.003
0.002
0.001
0.000
*
w1118
Mettl5 1bp/+
C
24-hour-sleep curve
Sleep Amount/30 mins
ZT0
ZT12
ZT24
D
total sleep
ZT0-ZT12(min)
ZT12-ZT24(min)
***
***
ns
*
**
Mettl5Gal4/+
UAS-Trmt112RNAi/+
UAS-Trmt112RNAi/Mettl5Gal4
E
sleep bout duration
ZT0-ZT12(min)
ZT12-ZT24(min)
*
ns
F
number of sleep bouts
N(ZT0-ZT12)
N(ZT12-ZT24)
G
awake % at ZT14
B
18S rRNA
m6A relative quantity
0.0025
0.0020
0.0015
0.0010
0.0005
0.0000
H
24-hour-sleep curve
I
total sleep
J
sleep bout duration
K
number of sleep bouts
L
awake % at ZT14
Mettl5Gal4>UAS-Mettl5m,Mettl5 1bp

Figure 3

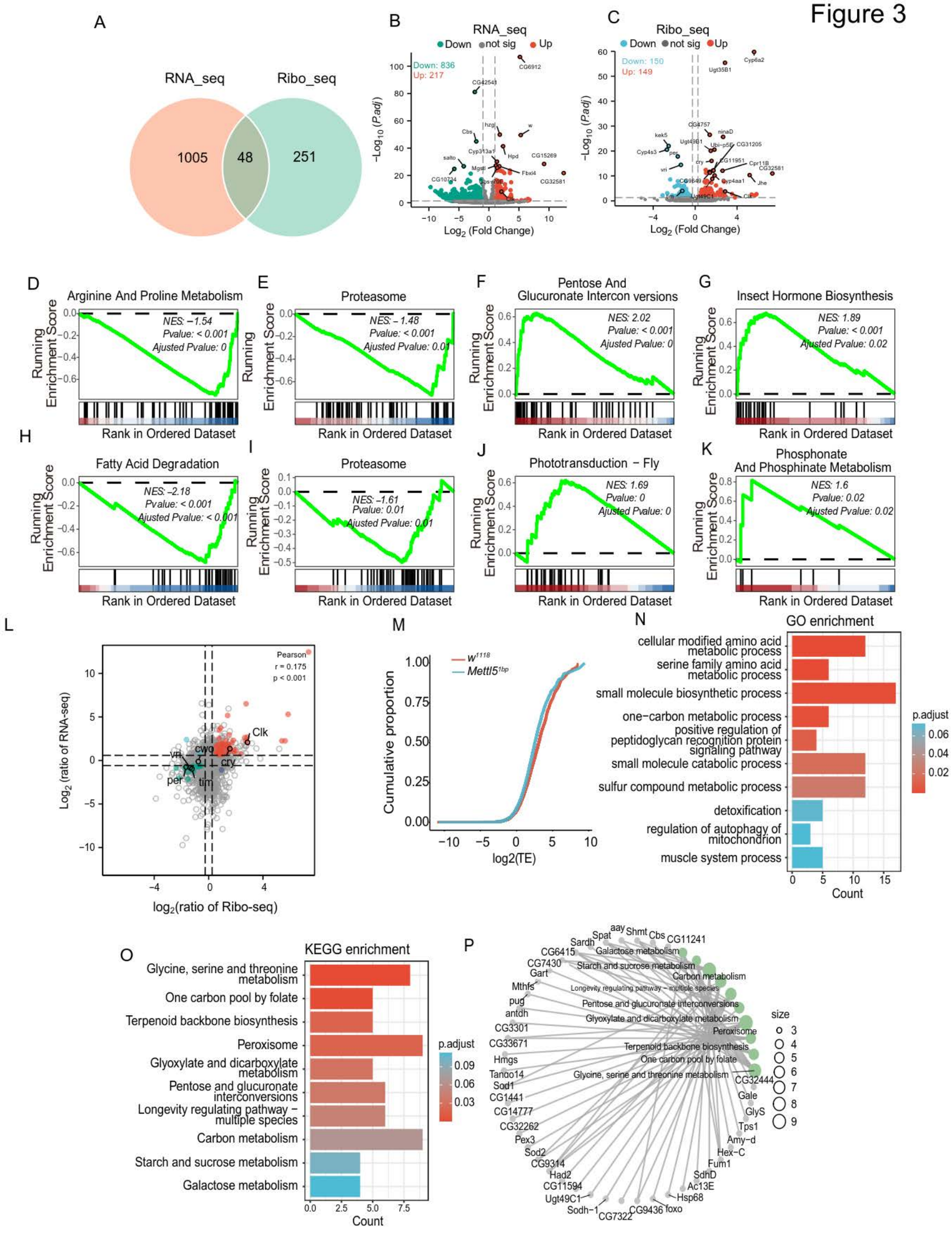
A
RNA_seq
Ribo_seq
1005
48
251
B
RNA_seq
Down
not sig
Up
Down: 836
Up: 217
CG6912
CG42541
hzg
w
Cbs
Cyp313a1
Hpd
CG15269
salto
Mgstl
Fbxl4
CG10734
CG32581
Clk
−Log10 (P.adj)
Log2 (Fold Change)
C
Ribo_seq
Down
not sig
Up
Down: 150
Up: 149
Cyp6a2
Ugt35B1
CG4757
ninaD
kek5
Ugt49B1
Ubi-p5E
CG31205
Cyp4s3
per
cry
CG11951
Cpr11B
CG32581
vri
CG9648
Cyp4aa1
Jhe
Clk
−Log10 (P.adj)
Log2 (Fold Change)
D
Arginine And Proline Metabolism
NES: −1.54
Pvalue: < 0.001
Ajusted Pvalue: 0
E
Proteasome
NES: − 1.48
Pvalue: < 0.001
Ajusted Pvalue: 0.01
F
Pentose And Glucuronate Intercon versions
NES: 2.02
Pvalue: < 0.001
Ajusted Pvalue: 0
G
Insect Hormone Biosynthesis
NES: 1.89
Pvalue: < 0.001
Ajusted Pvalue: 0.02
H
Fatty Acid Degradation
NES: −2.18
Pvalue: < 0.001
Ajusted Pvalue: < 0.001
I
Proteasome
NES: −1.61
Pvalue: 0.01
Ajusted Pvalue: 0.01
J
Phototransduction − Fly
NES: 1.69
Pvalue: 0
Ajusted Pvalue: 0
K
Phosphonate And Phosphinate Metabolism
NES: 1.6
Pvalue: 0.02
Ajusted Pvalue: 0.02
Running Enrichment Score
Rank in Ordered Dataset
L
Pearson
r = 0.175
p < 0.001
Clk
cwo
vri
cry
per
tim
Log2 (ratio of RNA-seq)
log2(ratio of Ribo-seq)
M
w1118
Mettl5 1bp
Cumulative proportion
log2(TE)
N
GO enrichment
cellular modified amino acid metabolic process
serine family amino acid metabolic process
small molecule biosynthetic process
one−carbon metabolic process
positive regulation of peptidoglycan recognition protein signaling pathway
small molecule catabolic process
sulfur compound metabolic process
detoxification
regulation of autophagy of mitochondrion
muscle system process
p.adjust
Count
O
KEGG enrichment
Glycine, serine and threonine metabolism
One carbon pool by folate
Terpenoid backbone biosynthesis
Peroxisome
Glyoxylate and dicarboxylate metabolism
Pentose and glucuronate interconversions
Longevity regulating pathway − multiple species
Carbon metabolism
Starch and sucrose metabolism
Galactose metabolism
p.adjust
Count
P
aay
Shmt
Cbs
CG11241
Spat
Sardh
CG6415
Galactose metabolism
CG7430
Starch and sucrose metabolism
Gart
Carbon metabolism
Mthfs
Longevity regulating pathway − multiple species
pug
Pentose and glucuronate interconversions
antdh
Glyoxylate and dicarboxylate metabolism
CG3301
Peroxisome
CG33671
Terpenoid backbone biosynthesis
Hmgs
One carbon pool by folate
Tango14
Glycine, serine and threonine metabolism
Sod1
CG32444
CG1441
Gale
CG14777
GlyS
CG32262
Tps1
Pex3
Amy-d
Sod2
Hex-C
CG9314
Fum1
Had2
SdhD
CG11594
Ac13E
Ugt49C1
Hsp68
Sodh-1
CG9436
foxo
CG7322
size

Figure 4

Differential expression of clock genes

A

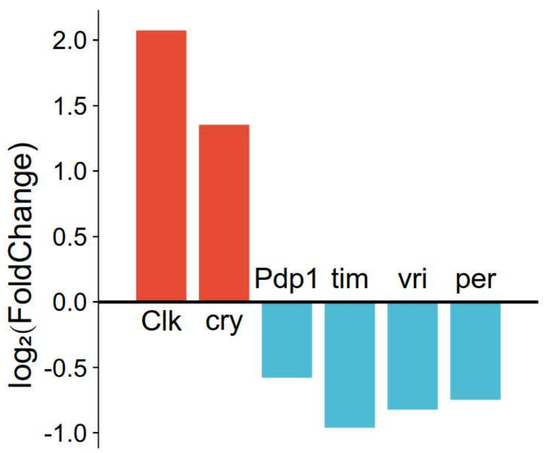

B

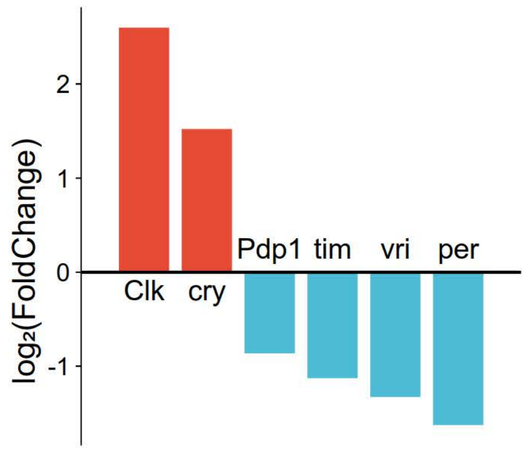

C

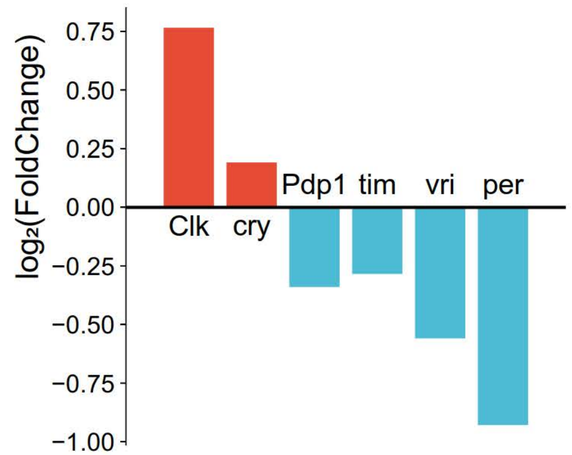

Differential expression of ribosome subunit

N

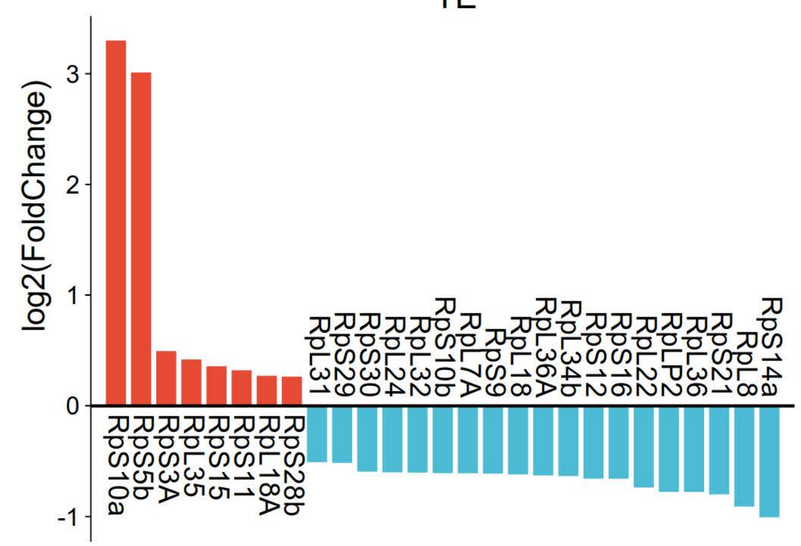

PER protein levels

D

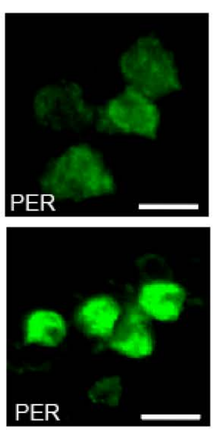

E

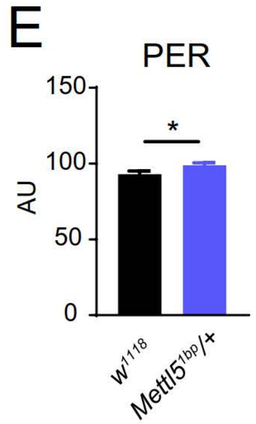

F

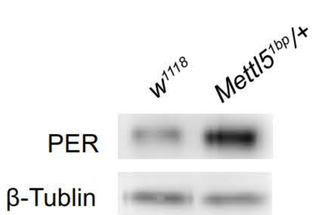

G

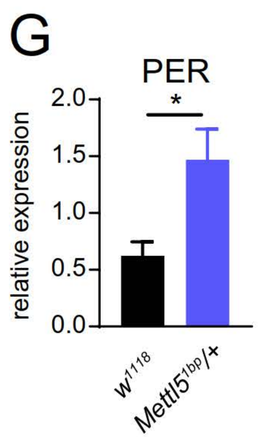

Genetic interactions

H

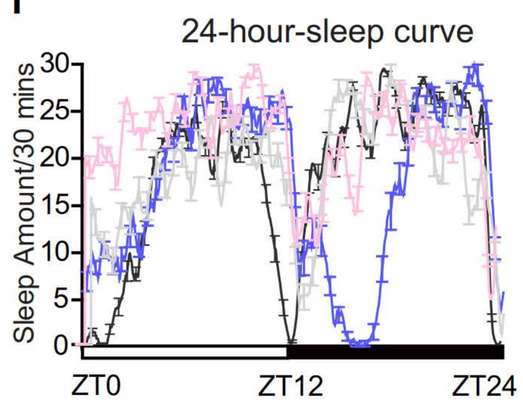

I

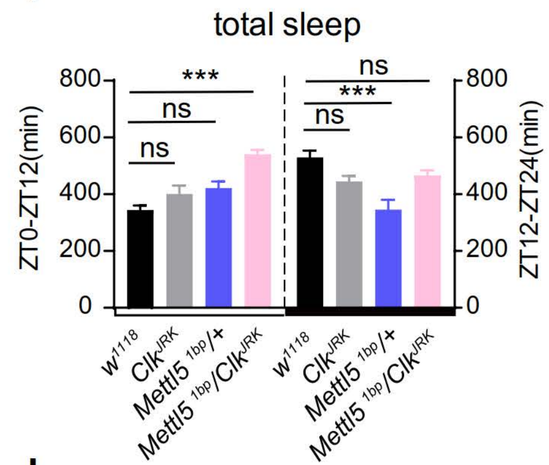

G

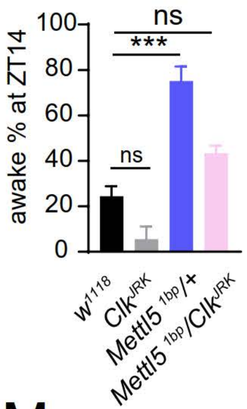

K

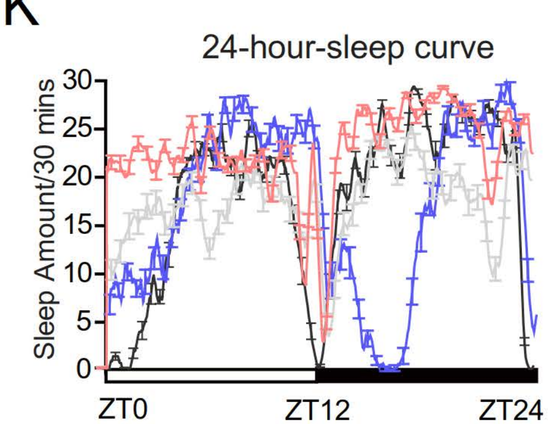

L

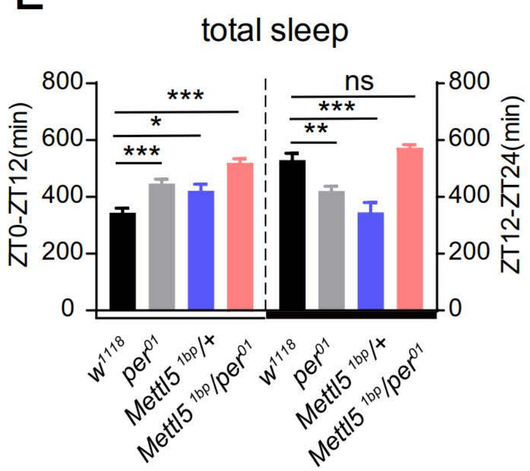

M

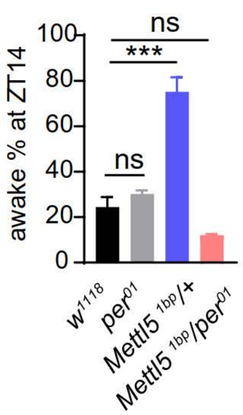

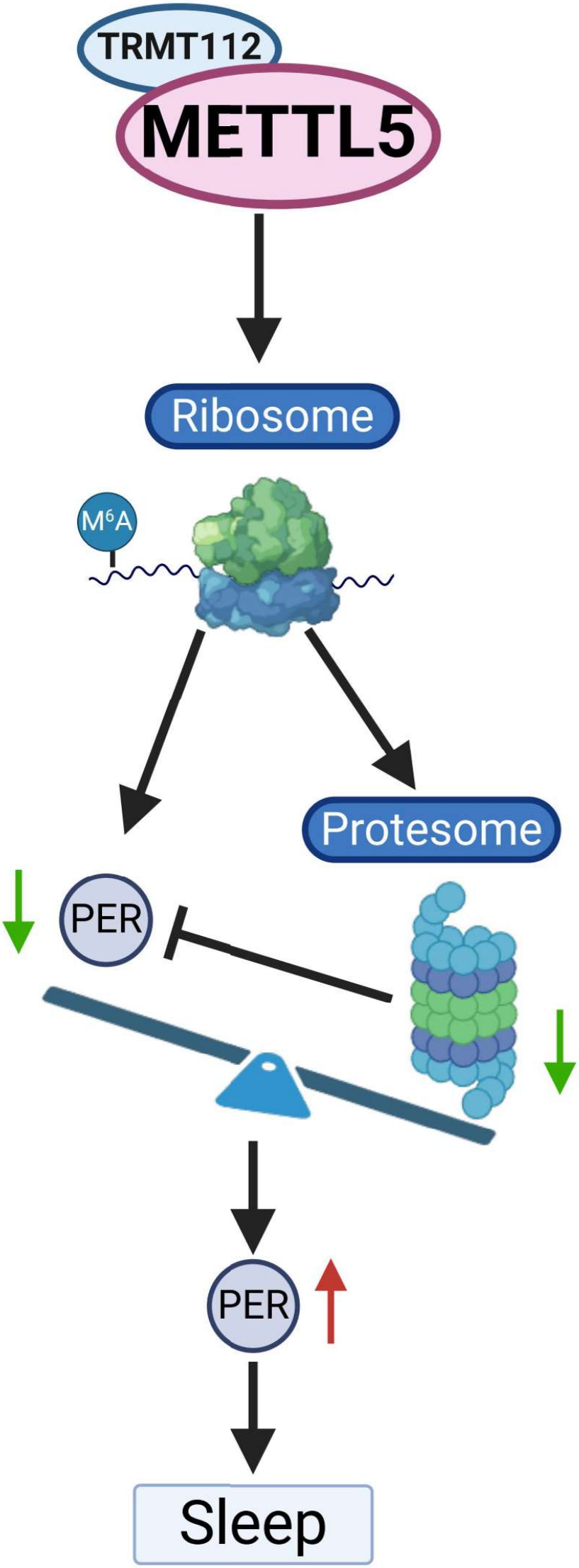
TRMT112
METTL5
Ribosome
M6A
Protesome
PER
PER
Sleep

Figure 6

UAS-DenMark,UAS-*syt*.GFP/+;*pdf*-GAL4/+

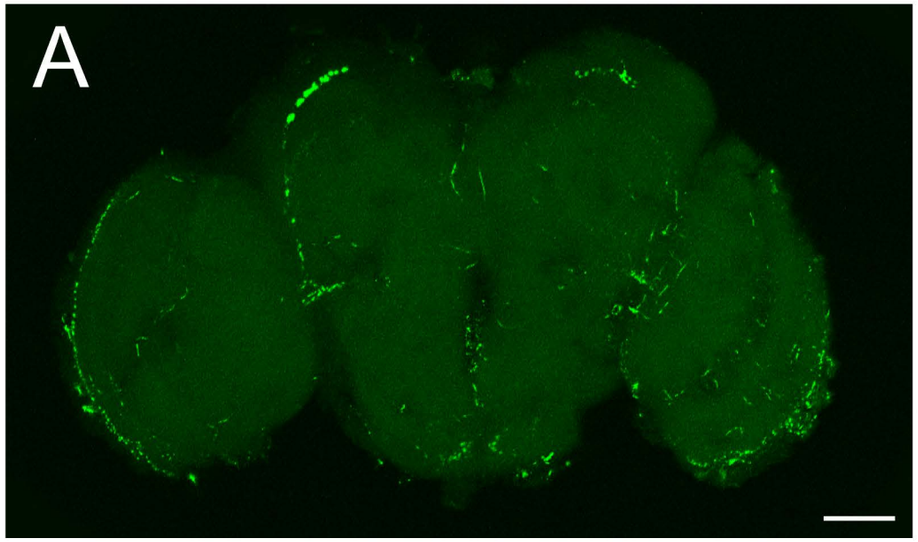

UAS-DenMark,UAS-*syt*.GFP/+;*pdf*-GAL4/UAS-*Fmr1*

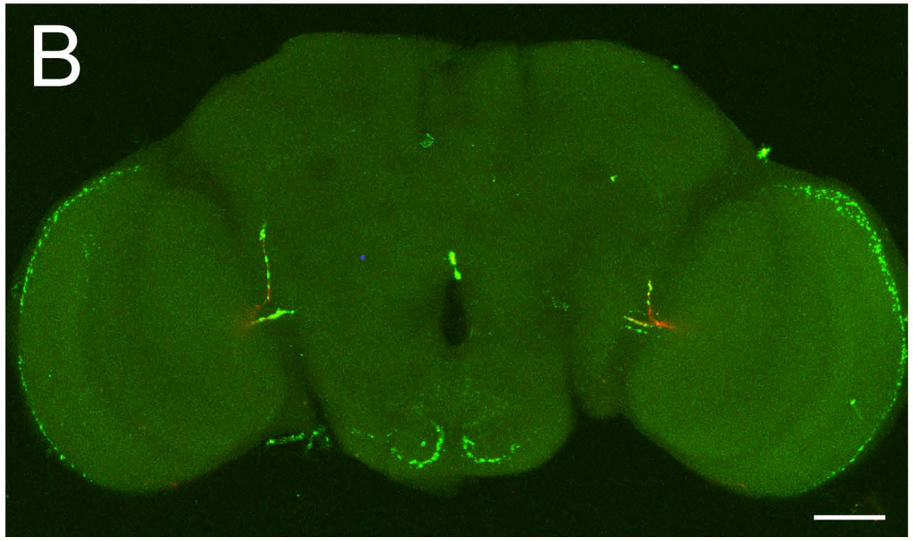

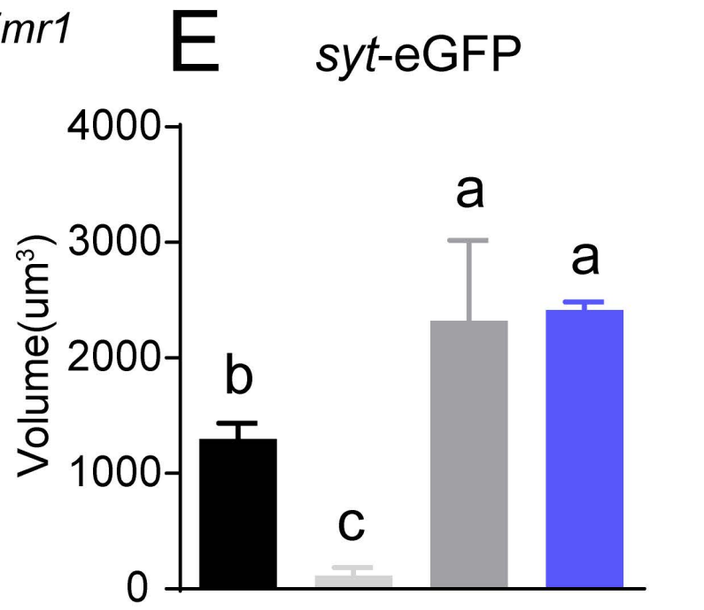

UAS-DenMark,UAS-*syt*.GFP/+;*pdf*-GAL4/*Fmr1*$^{\blacktriangle 50m}$

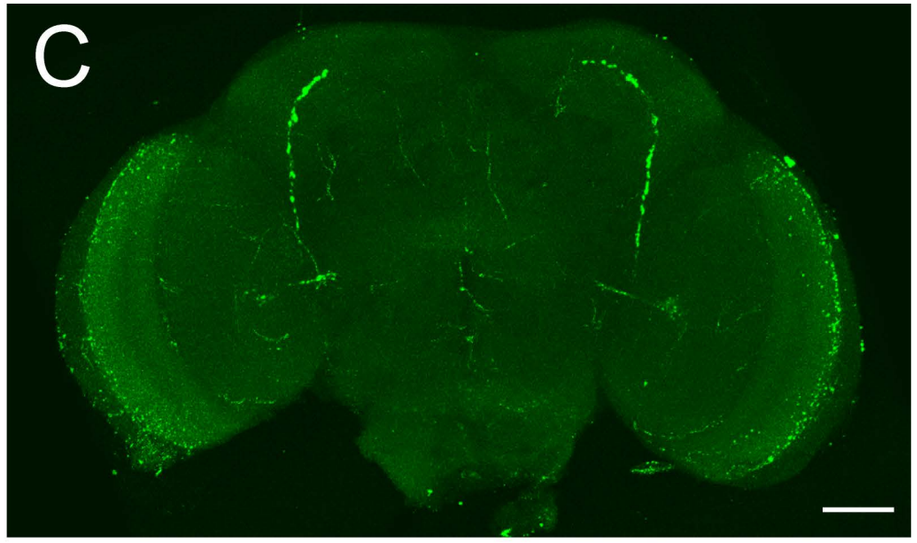

UAS-DenMark,UAS-*syt*.GFP/+;*pdf*-GAL4/*Mettl5*^{1bp}

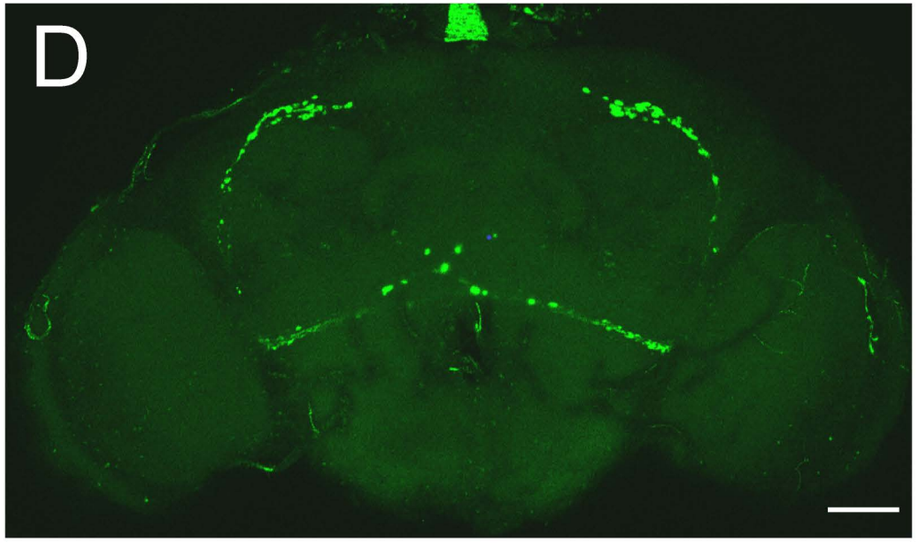

UAS-DenMark,UAS-*syt*.GFP/+;*pdf*-GAL4/+

UAS-DenMark,UAS-*syt*.GFP/+;*pdf*-GAL4/UAS-*Fmr1*

UAS-DenMark,UAS-*syt*.GFP/+;*pdf*-GAL4/*Fmr1*$^{\blacktriangle 50m}$

UAS-DenMark,UAS-*syt*.GFP/+;*pdf*-GAL4/*Mettl5*^{1bp}